

Supporting Information

**Controllable synthesis of flower-like hierarchical porous
TiO₂ at room temperature and its affinity application in
molecule with phosphate groups**

Jin-Hua Xu,^a Wen-Min Zhang,^b Hui Chen,^a Qing-Qing Ding,^a Shi-Ye Xie,^a Lan
Zhang^{a*}

^a Ministry of Education Key Laboratory for Analytical Science of Food Safety and
Biology, Fujian Province Key Laboratory of Analysis and Detection Technology for
Food Safety, College of Chemistry, Fuzhou University, Fuzhou, Fujian, 350116,
China

^b Department of Chemistry and Biotechnology, Minjiang Teachers College, Fuzhou,
Fujian, 350108, China

* Corresponding authors: Lan Zhang

E-mail addresses: zlan@fzu.edu.cn

Table of Contents

Table of Contents.....	2
1. Experimental section.....	3
1.1 Synthesis of TiO ₂ with different morphologies and structures.....	3
1.2 Computational method.....	4
1.3 Preparation of real samples	4
1.4 Selectivity study.....	5
2. Data.....	6
Table S1 Chemical structure of organophosphorus and parameters of GC-MS/MS.....	6
Table S2 Pore content of different size FHP-TiO ₂	7
Table S3 Calibration equation, limit of detection (LOD) and limit of quantitation (LOQ)	8
Table S4 Comparison with other reported adsorbents.	9
Table S5 Detection of organophosphorus in leek samples by FHP-TiO ₂ coupled with GC-MS/MS.....	10
Figure S1. TEM images of different dosage of resin.	11
Figure S2. TEM images of different stirring speed.....	12
Figure S3. TEM images of different ammonia content.	13
Figure S4. TEM images of different water amount.....	14
Figure S5. TEM images of different oxidation method.	15
Figure S6. TEM images of different initiating condition and strong acid etching.	16
Figure S7. TEM images of different oxidation time.	17
Figure S8. TEM images of different oxidation temperature.	18
Figure S9. Image of FHP-TiO ₂ before and after oxidation.	19
Figure S10. Application performance of FHP-TiO ₂ before and after oxidation.	20
Figure S11. HR-TEM images of the FHP-TiO ₂ 's lattice spacing.	21
Figure S12. TEM image of assembly nanosphere with different etch.	22
Figure S13. TEM image of assembling in different time.	23
Figure S14. Pore size distribution of different morphologie FHP-TiO ₂ by mercury intrusion method.	24
Figure S15. TEM image of different size FHP-TiO ₂	25
Figure S16. (a) N ₂ adsorption-desorption isotherms of different size FHP-TiO ₂ , (b) pore size distribution of different size FHP-TiO ₂ , (c) linear fitting of the specific surface area of different sizes FHP-TiO ₂ , (d) the loading of target in different size FHP-TiO ₂	26
Figure S17. Dynamic Light Scattering of different size FHP-TiO ₂	27
Figure S18. Pore size distribution of different size FHP-TiO ₂ by mercury intrusion method.....	28
References.....	29

1. Experimental section

1.1 Synthesis of TiO₂ with different morphologies and structures

Hollow dendritic TiO₂ were synthesized via a surfactant-free one-pot process according to report with some modifications.¹ In a typical synthesis, resin (0.20 g) and formaldehyde (37 wt%, 0.28 mL) were added to the solution composed of ammonia aqueous solution (28 wt%, 3.00 mL), deionized water (20 mL) and ethanol (60 mL). The mixture was vigorously stirred for 6 h at room temperature, then 0.6 mL of TBOT was added into the solution and stirred for 8 minutes before another addition of resorcinol (0.40 g) and formaldehyde (37 wt%, 0.56 mL). The mixture was stirred for another 2 h at room temperature, and then transferred into Teflon lined autoclave for hydrothermal treatment at 150 °C for 24 h. Then the as synthesized composites were collected by centrifugation, ethanol washing and drying at 50 °C. Finally, hollow dendritic TiO₂ were harvested after calcination at 550 °C for 5 h in air.

Rough surface TiO₂ were synthesized under similar process as illustrated above, resorcinol (0.20 g) and formaldehyde (37 wt%, 0.28 mL) were polymerized in ethanol/water/ammonia solution as described above for 18 h at room temperature, then 0.60 mL of TBOT was added for reaction of another 2 h. No hydrothermal treatment is needed here, the solid product was collected by centrifugation and then dried for calcination.

Mesoporous TiO₂ microspheres were synthesized according to report by the evaporation-driven oriented assembly (EDO) approach.² In summary, Pluronic F127 (PEO106PPO70PEO106, weight-average molecular weight = 12,600 g/mol), water, acetic acid, concentrated HCl (36 wt%), and TBOT were vigorously stirred in THF solvent to form a clear, golden yellow solution. Sequentially, the obtained clear solution was transferred into a volumetric flask and left in a drying oven to evaporate the THF solvent at 40 °C for 8 h, then at 80 °C for another 12 h to completely remove the solvent. Finally, the white TiO₂ mesoporous powder was obtained by calcination in air at 450 °C for 3 h. The detailed methods and characterization are available in the Supplementary Materials.

The flower-like SiO₂ were synthesized according to report by an epitaxial growth approach using cationic surfactant as a template, TEOS as a silica source, NaOH as a catalyst and organic solvent such cyclohexane as the oil phase.³ Typically, 1.00 g of CTAB and 0.80 mL of NaOH (0.10 M) were added to 50 mL of water and stirred gently at 60 °C for 2 h in a round bottom flask, then 20 mL of TEOS in cyclohexane (20 v/v%) was added to the solution and kept at 60 °C with stirring for 48 h. The products were collected by centrifuging and washed by water and ethanol for several times. Finally, the virus-like nanoparticles were dispersed in 50 mL of acetone and refluxed at 50 °C for 12 h to remove CTAB templates. Then, the samples were washed with ethanol and dried in vacuum at 45 °C for 8 h.

1.2 Computational method

All the geometric parameters of the studied compounds have been fully optimized without any constraints using the global hybrid generalized gradient approximation by employing standard density functional theory (DFT) technique at B3LYP and lanl2dz level, which is suitable for titanium atoms in weak and medium-strength interaction systems.⁴ The 6-31+G(d) split valence basis set was used for the system during geometric optimization. All isomers were characterized as local minima by harmonic vibrational frequency analysis at the same theoretical level after optimization. The polarizable continuum model was employed to take the effect of solvent (water) into account.⁵ Binding energies were calculated to evaluate the binding strength between titanium atoms and various molecules and ions. Here, binding strength is defined as the difference between the zero-point-corrected energies of a complex and separate titanium atoms and molecule/ion entities. The counterpoise procedure, where the whole basis set was used for the subunit energy calculations, was used to eliminate the basis set superposition error (BSSE) effect.^{6, 7} All calculations were carried out using the Gaussian 16 software package. Dimensional plots of molecular structures were generated with GaussView.⁸

1.3 Preparation of real samples

Organophosphorus: The fresh leek was bought from local markets in Fu Zhou, Fujian Province. Before the extraction, the 10 g of leek was homogenized with 20.00

mL of acetonitrile using a high-speed blender for 3 min. Then 3 g of NaCl was added into high-speed blender to homogenize for 3 min. The homogenized sample was centrifuged at 3000 rpm for 5 min to collect the supernatant for further use.

PS36:2: 1) Conventional pre-treatment: PS36:2 was extracted based on the method described by Huang et al.,⁹ 1.00 mL plasma was transferred into a 20 mL Eppendorf tube. The plasma was added with 10 mL of CHCl₃/CH₃OH (v/v = 1:1). The mixture was then added with 0.45 mL deionized water and vortexed followed by centrifugation at 12000 rpm for 10 min at 4 °C. The bottom layer containing phospholipids was collected and the top layer was subjected to the same extraction procedure. The samples collected from the two extractions were pooled and re-dissolved in 1.00 mL CHCl₃/CH₃OH (v/v = 1:1) after removing the solvent for HPLC-UV analysis.

2) Pretreatment with flower-like hierarchical porous nano-TiO₂: 3 mg of the FHP-TiO₂ was added to 10 mL of 10-fold diluted rat plasma (containing 0.40% acetic acid). After incubation for 10 min, the supernatant was discarded, while the FHP-TiO₂ was collected and then was further eluted with 1.00 mL of ammonia (0.80 wt%). Finally, the eluate was further analyzed by HPLC-UV.

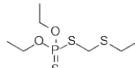
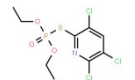
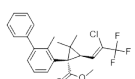
1.4 Selectivity study

Organophosphorus: Bifenthrin (1.44*1.27*0.74 nm, LogP: 7.30) was the co-existed substance of phorate (1.17*0.88*0.36 nm, LogP: 3.67) and clorpyrifos (1.02*0.98*0.69 nm, LogP: 4.77) in leek, therefore the specific performance of FHP-TiO₂ was evaluated by using bifenthrin as disruptor.¹⁰

PS36:2: DG (0.94*3.42*2.03 nm, LogP: 16.47) was the co-existed substance of PS36:2 (1.76*3.43*2.15 nm, LogP: 11.76) in plasma, therefore the specific performance of FHP-TiO₂ was evaluated by using DG as interferent.¹¹

2. Data

Table S1 Chemical structure of organophosphorus and parameters of GC-MS/MS

Analytes	Ret. time (min)	MS/MS transitions	Collision energy (Ev)	Structure
Phorate	7.10	260→121*/75	10	
Chlorpyrifos	8.31	350.59→197*/314	15	
Bifenthrin	11.17	422.87→166*/141	15	

“*” for quantification.

Table S2 Pore content of different size FHP-TiO₂

Size (nm)	Porosity (%)	Total pore volume (cm ³ /g)	BET surface area (m ² /g)
400	63.51	0.79	853.84
350	58.92	0.71	631.71
270	56.30	0.61	453.45
203	57.26	0.66	294.41
150	51.68	0.57	192.83

Table S3 Calibration equation, limit of detection (LOD) and limit of quantitation (LOQ)

Analytes	Linear range ($\mu\text{g}/\text{kg}$)	R	LODs ($\mu\text{g}/\text{kg}$)	LOQs ($\mu\text{g}/\text{kg}$)
Phorate	0.15-500.00	0.9998	0.05	0.15
Chlorpyrifos	0.03-500.00	0.9988	0.01	0.03
PS36:2	10.00-400.00	0.9964	3.00	10.00

Table S4 Comparison with other reported adsorbents.

Analytes	Adsorbents	Pretreatment method	LODs ($\mu\text{g}/\text{kg}$)	Linear range ($\mu\text{g}/\text{kg}$)	Recovery (%)	Ref
Phorate	-	SDME-GC-MS	4.83	5.00-1000.00	92.0-107.0	26
	-	LLE-GC-MS	3.00	10.00-100.00	94.0-98.5	29
	FHP-TiO ₂	SPME-GC-MS	0.05	0.15-500.00	100.1-110.6	This work
Chlorpyrifos	-	SDME-GC-MS	8.29	10.00-1000.00	77.0-94.0	26
	SA-MNPs	DSPE-GC-MS	5.00	50.00-1000.00	98.7-107.8	30
	FHP-TiO ₂	SPME-GC-MS	0.01	0.03-500.00	100.0-111.5	This work
	-	LLE-UHPLC-MS	0.62	15.84-79.20	-	27
PS36:2	g-C ₃ N ₄	ECL	100 cells/mL	2.5×10^2 - 1.0×10^6 cells/mL	-	31
	FHP-TiO ₂	DSPE-HPLC	3.00	10.00-400.00	91.8-95.2	This work

“-” means the data was not provided.

Table S5 Detection of organophosphorus in leek samples by FHP-TiO₂ coupled with GC-MS/MS

Leak	Fortified concentration (µg/kg)		Found by this method (µg/kg)		Recoveries of this method (mean ± SD, n = 3, %)	
	Phorate	Chlorpyrifos	Phorate	Chlorpyrifos	Phorate	Chlorpyrifos
1	0 (Initial)	0 (Initial)	0.12±0.01	0.20±0.02	/	/
2	2.00	2.00	2.13±0.02	2.23±0.01	110.6±10.0%	111.5±7.8%
3	20.00	20.00	20.11±0.09	20.23±0.11	100.6±8.4%	101.1±9.1%
4	500.00	500.00	500.22±0.18	500.34±0.20	100.1±7.5%	100.0±7.9%

The recovery of each method was calculated by the formula: $C_{Found}/C_{Spiked} \times 100\%$.

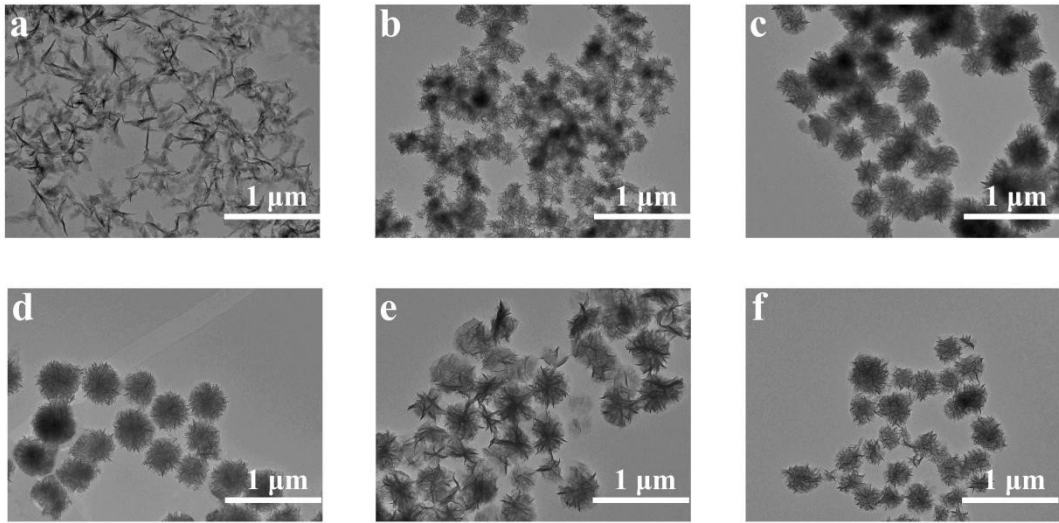


Figure S1. TEM images of different dosage of resin.

(a) 0.90 g, (b) 1.20 g, (c) 1.50 g, (d) 1.80 g, (e) 2.10 g, (f) 2.40 g.

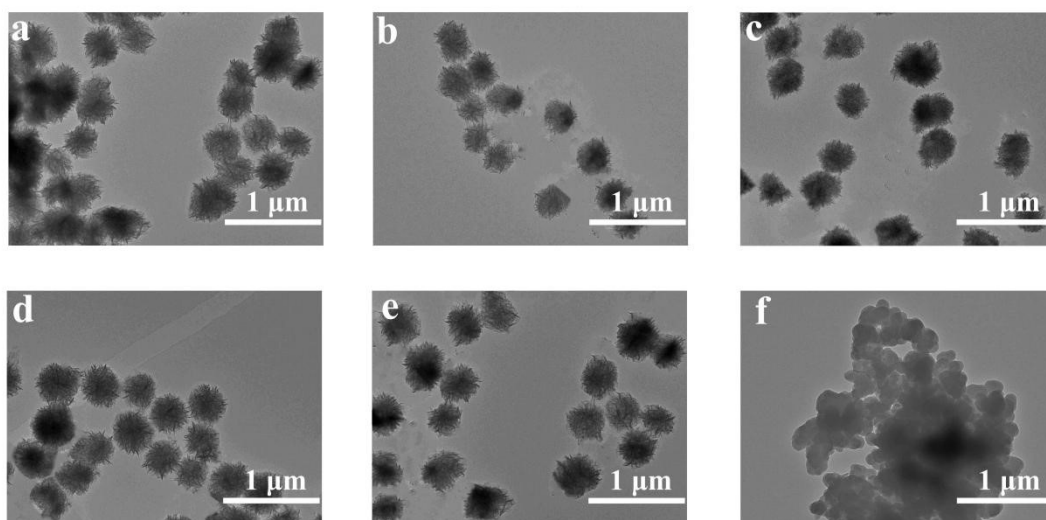


Figure S2. TEM images of different stirring speed.

(a) 300 rpm, (b) 600 rpm, (c) 900 rpm, (d) 1200 rpm, (e) 1500 rpm, (f) 1800 rpm.

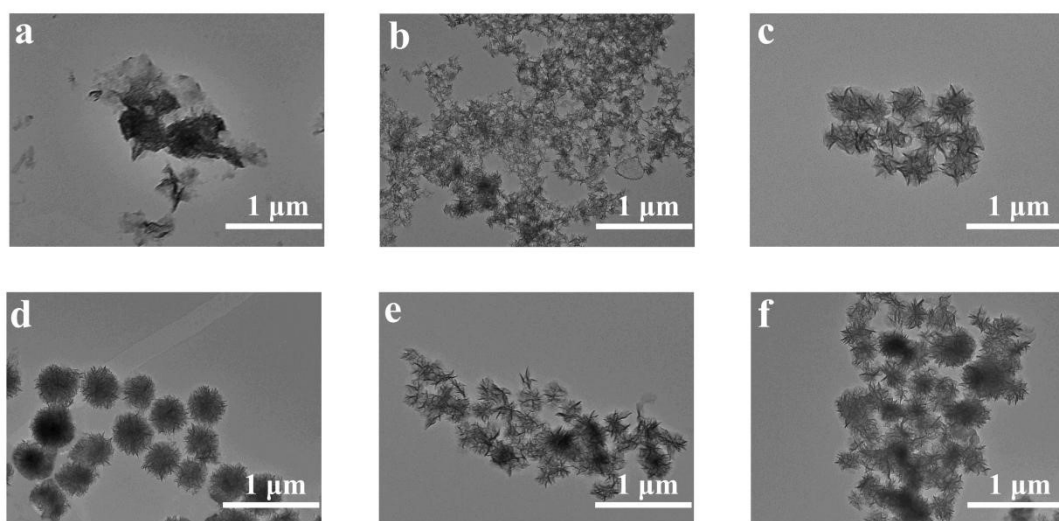


Figure S3. TEM images of different ammonia content.

(a) 0.00 mL, (b) 0.50 mL, (c) 1.00 mL, (d) 1.50 mL, (e) 2.00 mL, (f) 2.50 mL.

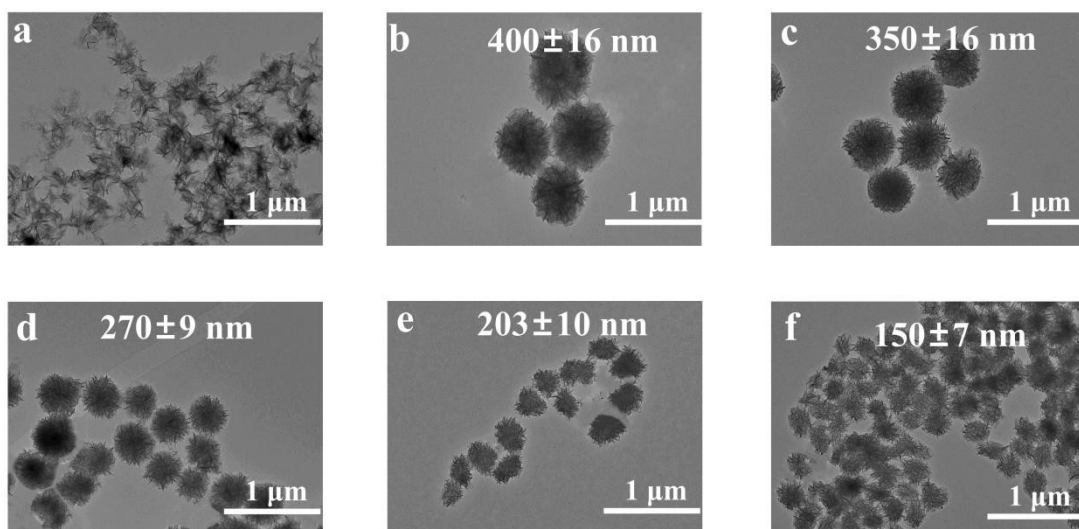


Figure S4. TEM images of different water amount.

(a) 0.00 mL, (b) 2.50 mL, (c) 5.00 mL, (d) 10.00 mL, (e) 15.00 mL, (f) 20.00 mL.

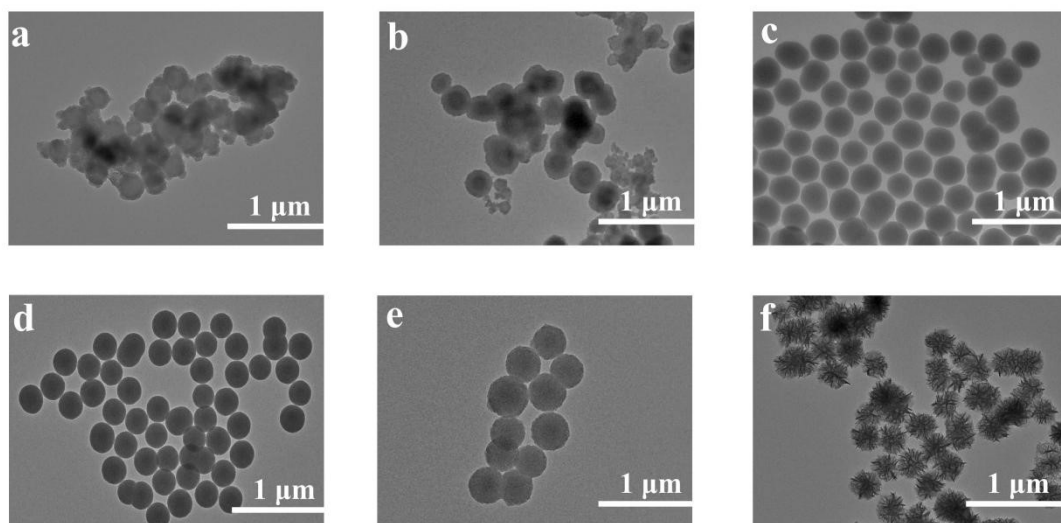


Figure S5. TEM images of different oxidation method.

(a) NaHCO_3 100 °C 1 h, (b) NH_4HCO_3 100 °C 1 h, (c) 100 °C 1 h, (d) KMnO_4 100 °C

1 h, (e) $\text{NH}_3 \cdot \text{H}_2\text{O}$ 100 °C 1 h, (f) H_2O_2 100 °C 1 h.

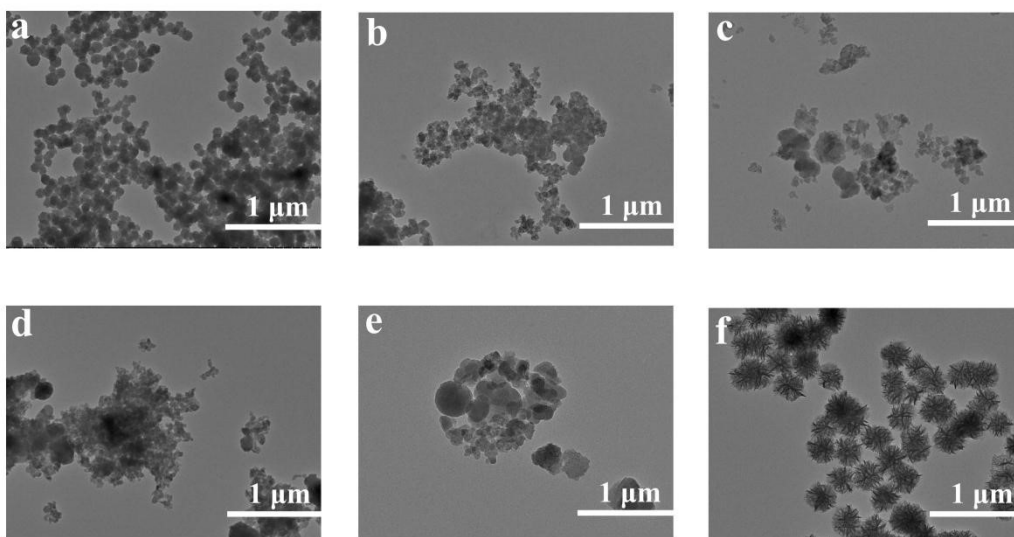


Figure S6. TEM images of different initiating condition and strong acid etching.

(a) UV+Fenton, RT, 12 h, (b) HCL, RT, 1 h, (c) $\text{H}_2\text{O}_2+\text{Fe}^{2+}$, RT, 1 h, (d) Fenton+hydrothermal reactor RT, 1 h, (e) H_2SO_4 , RT, 1 h, (f) H_2O_2 100 °C 1 h.

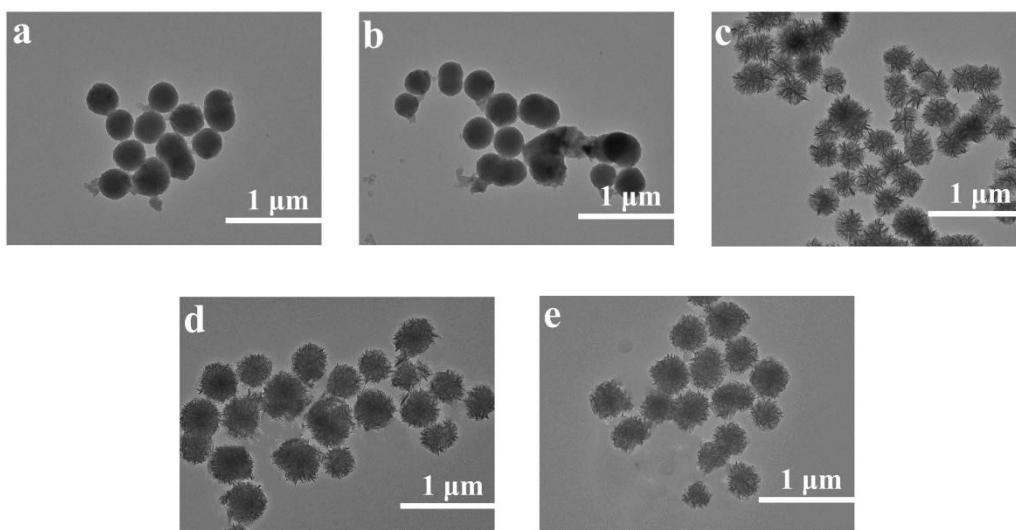


Figure S7. TEM images of different oxidation time.
(a) 30 min, (b) 45 min, (c) 60 min, (d) 90 min, (e) 120 min.

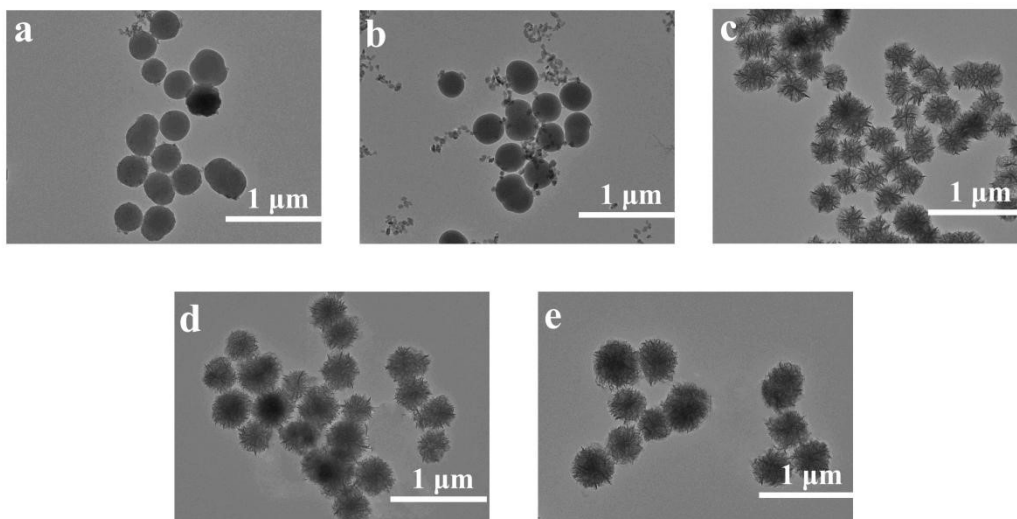


Figure S8. TEM images of different oxidation temperature.

(a) 60 °C, (b) 80 °C, (c) 100 °C, (d) 120 °C, (e) 140 °C.



Figure S9. Image of FHP-TiO₂ before and after oxidation.

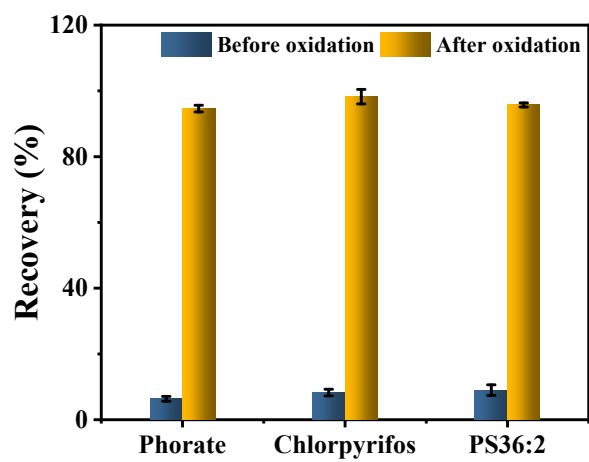


Figure S10. Application performance of FHP-TiO₂ before and after oxidation.

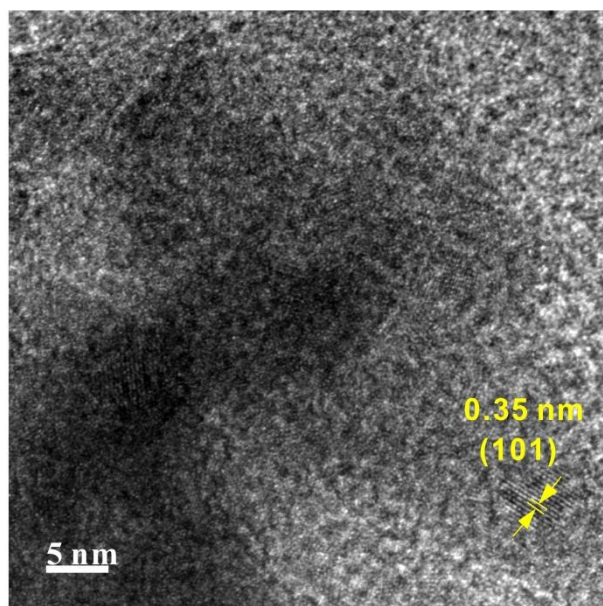


Figure S11. HR-TEM images of the FHP-TiO₂'s lattice spacing.

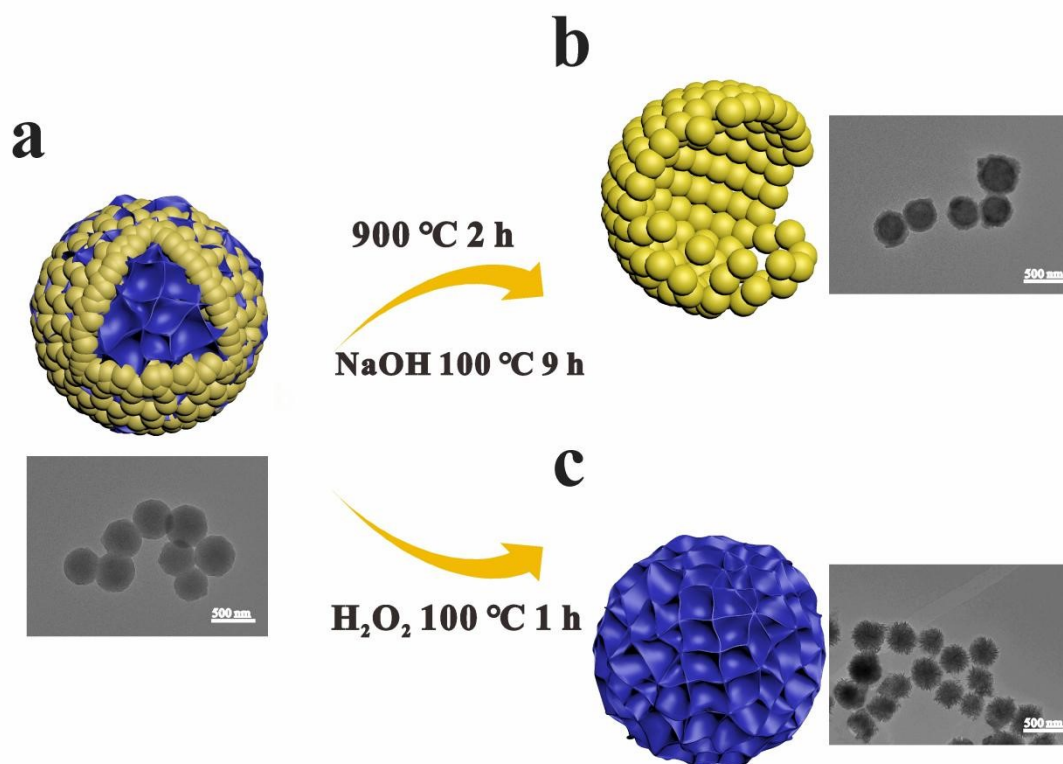


Figure S12. TEM image of assembly nanosphere with different etch. (a) TEM of without treatment, (b) TEM of after NaOH treatment, (c) TEM of after H₂O₂ oxidation.

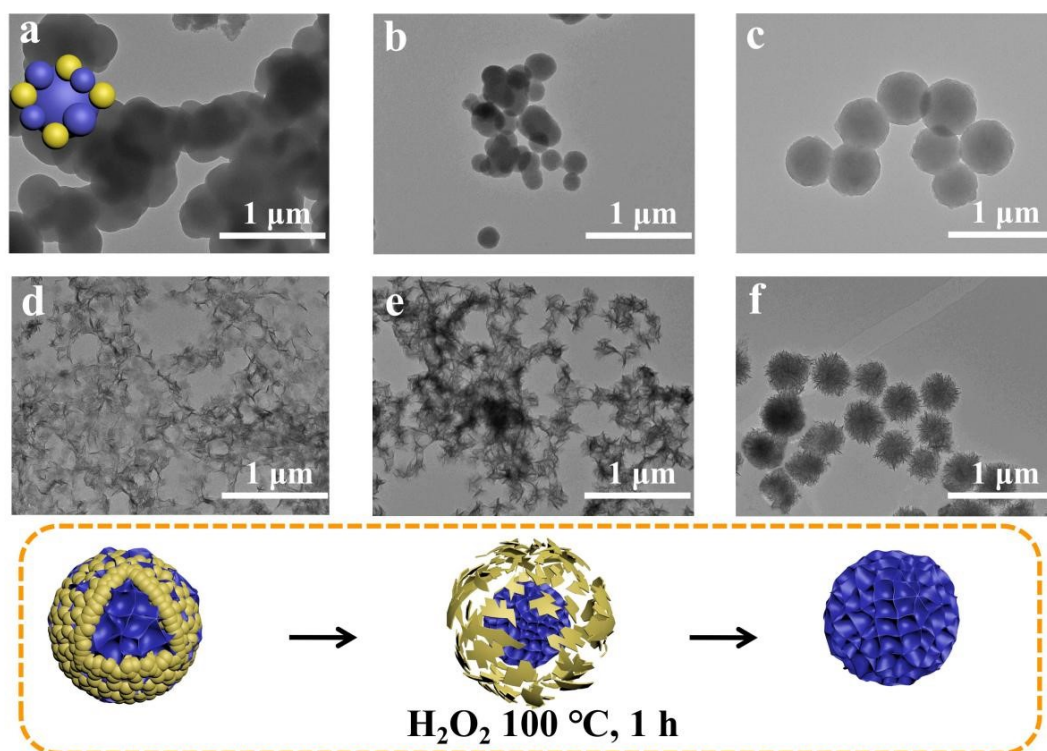


Figure S13. TEM image of assembling in different time.

(a) assembly 10 min without oxidation, (b) assembly 10 min with H_2O_2 oxidation, (c) assembly 30 min without oxidation, (d) assembly 30 min with H_2O_2 oxidation, (e) assembly 2 h without oxidation, (f) assembly 2 h with H_2O_2 oxidation.

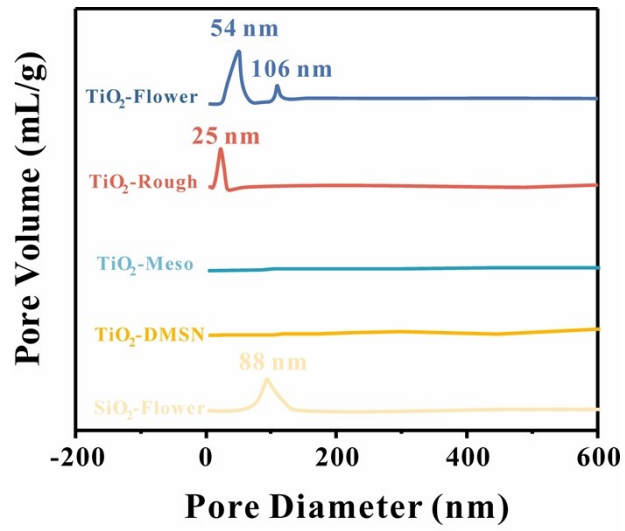


Figure S14. Pore size distribution of different morphologie FHP-TiO₂ by mercury intrusion method.

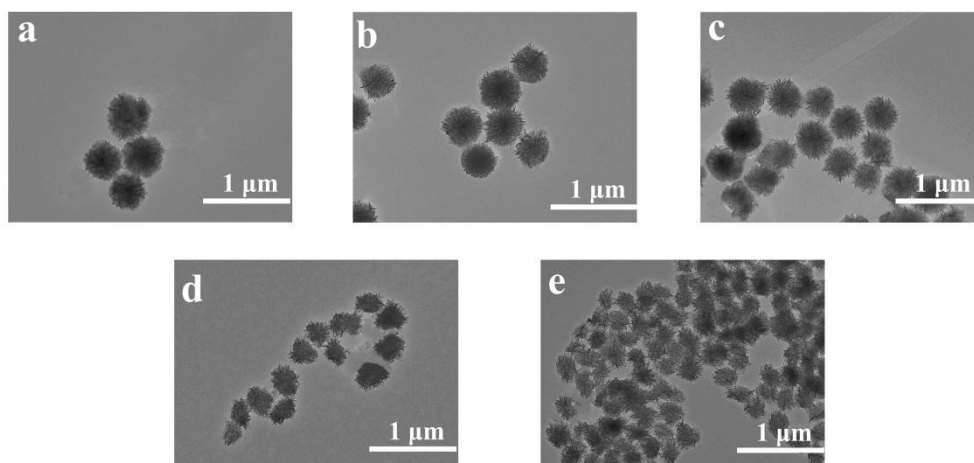


Figure S15. TEM image of different size FHP-TiO₂, (a) 2.50 mL 400 ± 16 nm, (b) 5.00 mL 350 ± 16 nm, (c) 10.00 mL 270 ± 9 nm, (d) 15.00 mL 203 ± 10 nm, (e) 20.00 mL 150 ± 7 nm.

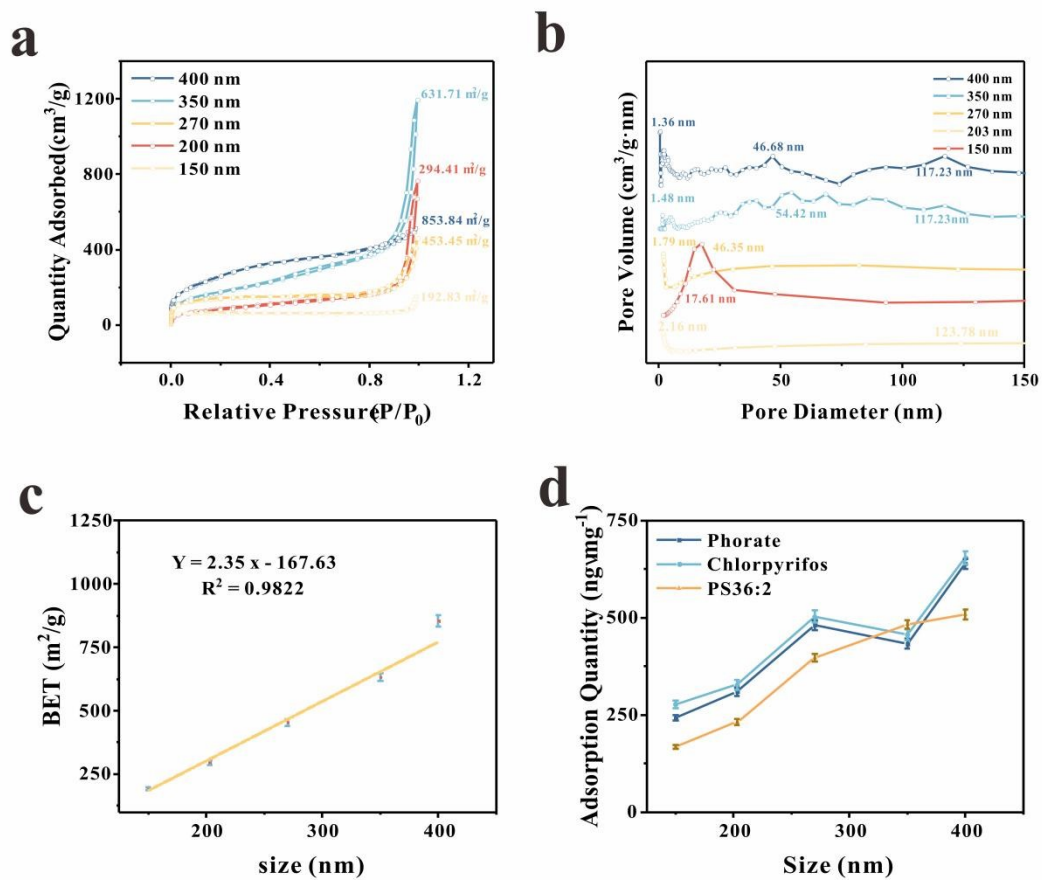


Figure S16. (a) N₂ adsorption-desorption isotherms of different size FHP-TiO₂, (b) pore size distribution of different size FHP-TiO₂, (c) linear fitting of the specific surface area of different sizes FHP-TiO₂, (d) the loading of target in different size FHP-TiO₂.

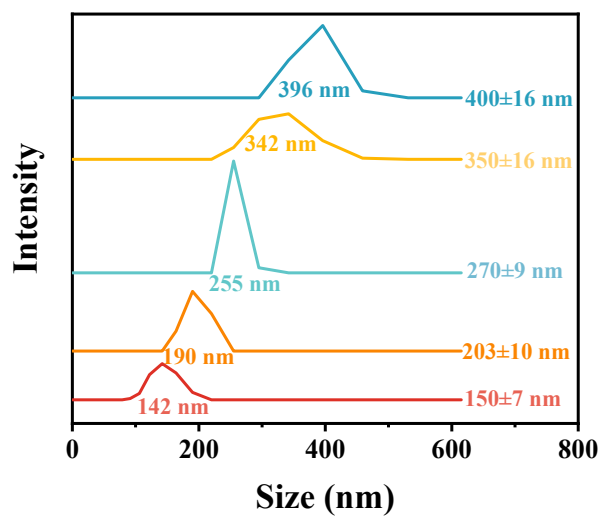


Figure S17. Dynamic Light Scattering of different size FHP-TiO₂.

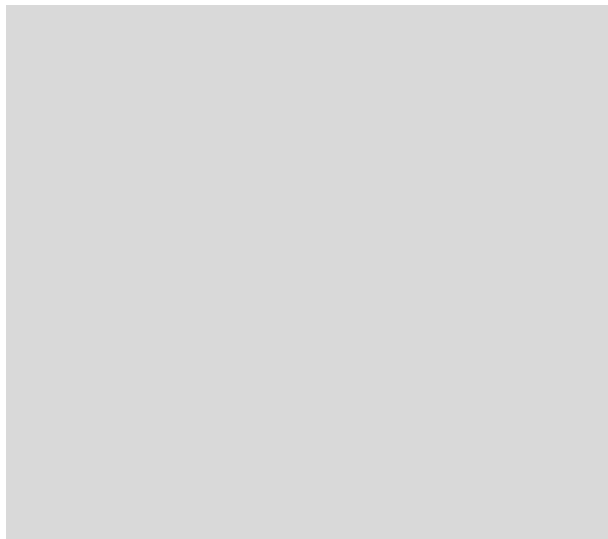


Figure S18. Pore size distribution of different size FHP-TiO₂ by mercury intrusion method.

References

- [1] H. Song, M. H. Yu, Y. N. Yang, J. Zhang, H. W. Zhang, C. Xu, N. Mitter, C. Z. Yu, *J Am Chem Soc.* **2016**, 138, 6455.
- [2] Y. Liu, R. C. Che, G. Chen, J. W. Fan, Z. K. Sun, Z. X. Wu, M. H. Wang, B. Li, J. Wei, D. Y. Zhao. *Sci Adv.* **2015**, 1, 4.
- [3] W. X. Wang, P. Y. Wang, X. T. Tang, A. Elzatahry, S. W. Wang, D. Al-Dahyan, M. Y. Zhao, C. Yao, C. T. Hung, X. H. Zhu, T. C. Zhao, X. M. Li, F. Zhang, D. Y. Zhao. *ACS Cent Sci.* **2017**, 3 (8), 839-846.
- [4] M. Rahmani, M. E. A. Benmalti, *J Biomol Struct Dyn.* **2022**, 40 (18), 8560-8568.
- [5] J. Tomasi, B. Mennucci, R. Cammi, *Chem. Rev.* **2005**, 105 (8), 2999-3093.
- [6] S. F. Boys, F. D. Bernardi, *Mol Phys.* **1970**, 19 (4), 553-556.
- [7] I. Alkorta, *Phys Chem.* **1999**, 103, 272-279.
- [8] Gaussian 16, Revision A.03, M. Frisch, G. Trucks, H. Schlegel, G. Scuseria, M. Robb, J. Cheeseman, G. Scalmani, V. Barone, G. Petersson, H. Nakatsuji, X. Li, M. Caricato, A. Marenich, J. Bloino, B. Janesko, R. Gomperts, B. Mennucci, H. Hratchian, J. Ortiz, A. Izmaylov, J. Sonnenberg, D. Williams-Young, F. Ding, F. Lipparini, F. Egidi, J. Goings, B. Peng, A. Petrone, T. Henderson, D. Ranasinghe, V. Zakrzewski, J. Gao, N. Rega, G. Zheng, W. Liang, M. Hada, M. Ehara, K. Toyota, R. Fukuda, J. Hasegawa, M. Ishida, T. Nakajima, Y. Honda, O. Kitao, H. Nakai, T. Vreven, K. Throssell, J. Montgomery, J. Peralta, F. Ogliaro, M. Bearpark, J. Heyd, E. Brothers, K. Kudin, V. Staroverov, T. Keith, R. Kobayashi, J. Normand, K. Raghavachari, A. Rendell, J. Burant, S. Iyengar, J. Tomasi, M. Cossi, J. Millam, M. Klene, C. Adamo, R. Cammi, J. Ochterski, R. Martin, K. Morokuma, O. Farkas, J. Foresman, and D. Fox, Gaussian, Inc., Wallingford CT, **2016**.
- [9] Q. Huang, H. Lei, M. Dong, H. Tang, Y. Wang, *Analyst.* **2019**, 144 (13), 3980-3987.
- [10] R. Dennington II, T. Keith and J. Millam, GaussView, version 6; Semichem, Inc. **2000-2016**.
- [11] J. Chen, Z. Guo, H. Zhang, Y. Xin, Y. Shi, Z. Gu, L. Zhang, J. Zhong, X. Guo, Y.

Li, *Chem Eng J.* **2022**, 446, 136933.